Theory of Single-Molecule Optical Line-Shape Distributions in Low-Temperature Glasses

Eitan Geva and J. L. Skinner*

Theoretical Chemistry Institute and Department of Chemistry, University of Wisconsin, Madison, Wisconsin 53706

Received: May 29, 1997; In Final Form: August 11, 1997[⊗]

We present a theoretical framework for analyzing the distribution of optical line shapes in low-temperature glasses, as measured by single-molecule spectroscopy. The theory is based on the standard tunneling two-level system model of low-temperature glasses and on the stochastic sudden jump model for the two-level system dynamics. Within this framework we present an explicit formula for the line shape of a single molecule and employ Monte Carlo simulation techniques to calculate the distribution of single-molecule line shapes. We compare our calculated line-width distributions to those measured experimentally. We find that the two-level system model captures the features of the experimental line-width distributions very well, although there are discrepancies for small line widths. We also discuss the relation of single-molecule line-shape distributions to more traditional "line shapes", as measured by hole-burning and photon echo spectroscopies. Using the results from our analysis of the single-molecule line-width distributions, with no adjustable parameters we can compare theoretical predictions with experiment for photon echo decay times and hole widths. In general, the agreement is good, providing further evidence that the standard tunneling model in glasses is basically correct. For two systems, however, theory and experiment do not agree quantitatively.

I. Introduction

The electronic energy levels of a chromophore embedded in a solid host are very sensitive to the chromophore's local environment. Hence, in principle, optical spectroscopy of dilute chromophores in solids can probe the microscopic structure and dynamics of the host.[1−5] Focusing on one specific transition of a single chromophore, the (angular) transition frequency $\omega(t)$ is a sum of a static (on the experimental time scale) component, ω_0, and a dynamic component, $\delta\omega(t)$. The static component sets the frequency origin for the spectral line, and the dynamic component determines the line shape. Solids always contain some degree of disorder, and so different chromophore molecules have different local environments. Different chromophore molecules will, therefore, in general, have different static and dynamic components of their transition frequencies. However, the distribution over the static component is typically much wider than the absorption line shape of each of the individual chromophore molecules. Typical absorption spectra, which measure the response of a very large number ($\sim 10^{15}$) of chromophores, are therefore completely dominated by the distribution of the static component, i.e., they are *inhomogeneously broadened*. This is particularly true in the case of amorphous hosts. Inhomogeneous broadening contains important information about structural disorder.[6−9] However, it also prevents the extraction of information on the host's dynamics. One must therefore resort to alternative techniques in order to unveil this important information.

Several *line-narrowing* spectroscopies have been developed in order to circumvent inhomogeneous broadening, namely hole-burning (HB)[2,3,10,11] and luminescence-line-narrowing[2,12] in the frequency domain, and two- and three-pulse photon echoes (PE)[13−21] in the time domain. These techniques indeed eliminate the inhomogeneous broadening, either by rephasing (in the time domain) or by selective narrow-band excitation of a small subset of the chromophores (in the frequency domain). Hence, they directly probe the dynamics that give rise to $\delta\omega(t)$. However, these line-narrowing techniques still involve a very large number of chromophore molecules and therefore measure an ensemble average of the host's fluctuations. A key question is whether or not information is lost by this averaging process. That is, if the dynamical fluctuation is the same, in a statistical sense, for each individual chromophore molecule, then the answer to this question is no. If, on the other hand, the dynamical fluctuations are different for each chromophore, then the answer is yes; information is indeed lost by the ensemble averaging inherent in traditional line-narrowing experiments.

In a crystal, $\delta\omega(t)$ results from coupling to acoustical, optical, and pseudo-local phonons.[22−24] The nature of the system is such that different chromophore molecules interact with exactly the same phonons. This is because the acoustic and optical phonons are delocalized throughout the crystal, and the pseudo-local phonons induced by each chromophore are identical. Ensemble averaging in this case therefore does not lead to any loss of information, and the resulting line shape is equivalent to that of a single molecule (the so-called "homogeneous line shape"). In a glass, at low temperatures, dynamical fluctuations are believed to be due to the *local* rearrangement of small groups of atoms. Since the glass is strongly disordered, these fluctuations are expected to differ from one chromophore molecule to the next. As a result, different chromophores will have different line shapes, which reflect the unique dynamics of their individual local environments. What line-narrowing spectroscopies really measure in glassy hosts are therefore averages over the distribution of dynamical fluctuations. Hence, since a distribution always contains more information than its average, the ensemble averaging inherent in traditional line-narrowing techniques leads to a considerable loss of information when applied to such disordered hosts.

The measurement of the distributions underlying the averages inherent in traditional line-narrowing techniques requires doing spectroscopy at the single molecule level. In fact, the optical spectroscopy of individual chromophores embedded in solids has recently become experimental reality.[25,26] This new and

[⊗] Abstract published in *Advance ACS Abstracts,* October 1, 1997.

S1089-5647(97)01722-7 CCC: $14.00

exciting field has been called single molecule spectroscopy (SMS) (for reviews see refs 5, 27−32). The measurement of the fluorescence excitation line shape of an individual impurity molecule is made possible by (1) selecting a photostable chromophore with a narrow zero-phonon line and high fluorescence yield, (2) exciting only a very small volume of the sample, (3) taking advantage of inhomogeneous broadening to selectively excite a single molecule at a time with a narrowband laser, and (4) using efficient fluorescence collection optics to detect the signal from the single molecule. SMS has been applied in recent years to an increasing number of systems, including crystals,[25,26,33−48] Shpol'skii matrices,[49−57] amorphous polymers,[58−60] and semicrystalline polymers.[61−68]

In this paper we focus on the distribution of single-molecule line widths in amorphous hosts at cryogenic temperatures. Such measurements have been performed on four amorphous polymeric hosts (polystyrene (PS), poly(methyl methacrylate) (PMMA), polyvinylbutyral (PVB),[58] and polyisobutylene (PIB)[59,60]) and one semicrystalline (partly amorphous) polymeric host (polyethylene (PE)[59,60,64]). In each case wide distributions of line widths have been found. As mentioned above, these line-width distributions are the direct result of the fact that different chromophore molecules experience different (in a statistical sense) dynamics in their local environments. These line-width distributions therefore allow us to glimpse for the first time into the distributions that underly the averages measured by traditional line-narrowing techniques. They provide insight into how these averages are related to the distribution, and more importantly, they contain new information about the nature of glass dynamics. These exciting experiments have received only limited theoretical attention.[64]

Glasses are of great technological importance, and they are fundamentally fascinating in their own right. The anomalous behavior of glasses at low temperature (as compared to crystals), as well as its universal nature (independent of the chemical composition of the glass), have puzzled researchers since their discovery (for reviews see refs 69−72). Unlike crystals, whose low-temperature properties are dominated by phonons, glasses contain what appear to be additional excitations that arise from local structural dynamics. These additional excitations give rise to such anomalies as an excess specific heat that is more or less linear in temperature and depends logarithmically on the experimental time scale,[73,74] a heat conductivity that is roughly quadratic in temperature,[73,75] an ultrasonic attenuation that is linear in temperature for small acoustic frequencies,[76−79] and optical photon echo decay rates and hole widths that are more or less linear in temperature and logarithmic in the experimental time scale.[4,5,80] Additional anomalies have been observed in other thermal, acoustical, and electrical properties.[69−72]

Twenty five years after its first discovery, a fundamental understanding of the microscopic source for the low-temperature glass anomaly and its universality is still missing.[81] However, there exists a relatively simple phenomenological model that appears to be consistent with most experimental observations to date. This model, independently proposed by Anderson, Halperin, and Varma[82] and Phillips,[83] links the additional glass excitations to tunneling within double-well features in the multidimensional potential energy surface of the glass. The description of each double well is then further reduced to a two-level system (TLS), and the glassy disorder is expressed by introducing distributions of the TLS parameters. This reduced description of the glass as a collection of tunneling TLSs turns out to be surprisingly successful in accounting for the anomalous thermal,[73,82,83] acoustical,[76−79,84−86] electrical,[86] and optical properties of low-temperature glasses.[4,5,80,87]

The formalism used in the analysis of optical PE and HB experiments in low-temperature glasses has its roots in magnetic resonance theory. The analysis is based on the stochastic sudden jump model pioneered by Klauder and Anderson.[88] The sudden jump model first penetrated the field of low-temperature glasses in the context of explaining their anomalous *acoustic* properties.[77,89−91] The analogy between the TLS−TLS interaction, which is important in understanding the acoustic properties, and the interaction between a TLS and an optically active chromophore then led to its application in the analysis of optical experiments.[4,80,92−102]

In this paper we present a theoretical framework for analyzing the distribution of line widths as measured by SMS in low-temperature glasses in terms of the TLS and stochastic sudden jump models. (A brief preliminary account of some aspects of this work has already appeared.[103,104]) The theoretical model involves a number of parameters, only one of which, the TLS−chromophore coupling constant, cannot be estimated from independent sources. We compare our results to all of the available experimental single-molecule line width distribution data, and for each system we treat the TLS−chromophore coupling as an adjustable parameter. Once this parameter is known, we then calculate echo decay times and hole widths, without any adjustable parameters. Thus the comparison of PE, HB, and SMS experimental data, with the same basic theoretical model and the same parameters, provides a discriminating test of the TLS model. For the most part, the TLS model succeeds quite well. However, detailed comparisons of our theoretical line width distributions to the experimental ones, do show small but systematic discrepancies, as does comparison of the resulting no-adjustable-parameter theory with HB and PE results.

The paper is organized as follows. In section II we present and discuss in detail the TLS model of low-temperature glasses and the stochastic sudden jump model. An effort is made to present a self-contained description of the model, with emphasis on its application to the optical spectroscopy of dilute chromophores in glasses. In section III we outline the derivation of a formula for the line shape of a single molecule embedded in a glass. In section IV we discuss some new theoretical results for PE and HB observables,[105] which we need for comparison of SMS, PE and HB experiments. In section V we calculate the distribution of single-molecule line widths for six different systems, and in each case compare with experimental data. We also compare our PE and HB calculations to experimental results for the same systems. In section VI we conclude.

II. Two-Level System and Sudden Jump Models

Consider a chromophore embedded inside a glassy host at a low temperature (∼1 K). It is widely accepted, on the basis of thermal, acoustical, electrical, and spectroscopic experiments, that the only active degrees of freedom, under these conditions, except for acoustic phonons, correspond to localized and relatively small groups of glass atoms moving within double well features of the potential energy hypersurface.[69−72,82,83,106−108] The low temperature also allows for the description of each such double well in terms of its two lowest energy levels, i.e., as a TLS. These TLSs are coupled to the acoustic phonons of the glass, which induce flipping between the two states. The inherent disorder in glasses is then manifested by the distributions of the spatial locations, orientations, flipping rates, and energy splittings of the TLSs.

Consider a generic double well, as shown in Figure 1. It is convenient to present the Hamiltonian of the corresponding TLS in terms of a basis set consisting of two *localized* states, $|L\rangle$ and $|R\rangle$ (cf. Figure 1). It is convenient to choose the wave functions of both localized states to be real and positive.[109]

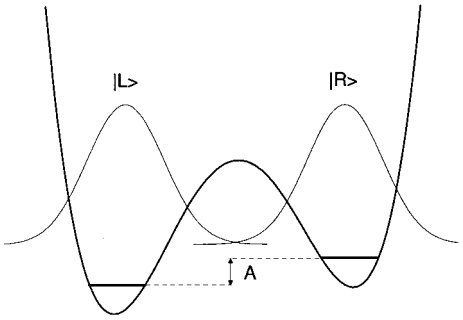

Figure 1. A double well. Also shown are the localized basis states, $|L\rangle$ and $|R\rangle$.

Within this localized representation, the Hamiltonian of the TLS is given by

$$\mathbf{H}_{\mathrm{TLS}} = A\mathbf{S}_z - J\mathbf{S}_x = {}^1/_2\begin{pmatrix} A & -J \\ -J & -A \end{pmatrix} \tag{1}$$

where, using spin $-{}^1/_2$ terminology, $\mathbf{S}_z = (|R\rangle\langle R| - |L\rangle\langle L|)/2$ and $\mathbf{S}_x = (|R\rangle\langle L| + |L\rangle\langle R|)/2$; A is the *asymmetry*, i.e., the energy gap between the localized states (the energy origin is conveniently set at the average of the energies of the localized states); and $J > 0$ is the *tunneling matrix element* that couples the two localized states. The asymmetry A may be negative or positive with equal probability since the underlying physics inflicts no asymmetry between the two sides of the barrier. By a suitable redefinition of the two states, we therefore can always assume that $A > 0$. It is also generally true that J is real and positive.[70,109]

A glassy medium is disordered on a microscopic scale. On a larger length scale, however, it behaves like a continuous elastic medium, as does a crystal. Glassy media can therefore support long-wavelength longitudinal and transverse acoustic phonons.[110] The TLSs are coupled to this thermal acoustic phonon bath. The TLS−phonon interaction is assumed weak so that only terms linear in the medium-density fluctuation[111] and the effective coordinate of the TLS are retained. This leads to the following interaction Hamiltonian:[109,112]

$$\mathbf{H}_{\mathrm{TLS,ph}} = \mathbf{S}_z \otimes \sum_i g_i\sqrt{\omega_i}(a_i + a_i^\dagger) \tag{2}$$

where g_i are coupling constants and ω_i, a_i, $a_i^\dagger$ are the angular frequency, annihilation, and creation operators of the ith normal mode, respectively. $\mathbf{H}_{\mathrm{TLS,ph}}$ is diagonal in the localized TLS representation since $\mathbf{S}_z$ is associated with the asymmetry of the double well, and is therefore linear, to first order, in its effective coordinate (cf eq 1).[70,109] Equations 1 and 2 are isomorphic to the extensively studied spin−boson Hamiltonian.[109,113]

The rate constant for phonon-assisted flipping of the TLS is evaluated in the limit of weak TLS−phonon coupling. We first transform to the eigenrepresentation of $\mathbf{H}_{\mathrm{TLS}}$. The eigenstates of $\mathbf{H}_{\mathrm{TLS}}$ are

$$\begin{aligned} |-\rangle &= \cos(\phi)|L\rangle + \sin(\phi)|R\rangle \\ |+\rangle &= -\sin(\phi)|L\rangle + \cos(\phi)|R\rangle \end{aligned} \tag{3}$$

where $\tan(2\phi) = J/A$. The corresponding eigenvalues are $\pm E/2$ with

$$E = \sqrt{A^2 + J^2} \tag{4}$$

such that $\mathbf{H}_{\mathrm{TLS}}|\pm\rangle = \pm(E/2)|\pm\rangle$. Equations 1 and 2 are then transformed into

$$\mathbf{H}_{\mathrm{TLS}} = E\tilde{\mathbf{S}}_z = {}^1/_2\begin{pmatrix} E & 0 \\ 0 & -E \end{pmatrix} \tag{5}$$

$$\mathbf{H}_{\mathrm{TLS,ph}} = \left(\frac{A}{E}\tilde{\mathbf{S}}_z + \frac{J}{E}\tilde{\mathbf{S}}_x\right) \otimes \sum_i g_i\sqrt{\omega_i}(a_i + a_i^\dagger) \tag{6}$$

where $\tilde{\mathbf{S}}_z = (|+\rangle\langle+| - |-\rangle\langle-|)/2$ and $\tilde{\mathbf{S}}_x = (|+\rangle\langle-| + |-\rangle\langle+|)/2$.

Within second-order perturbation theory, only the term linear in $\tilde{\mathbf{S}}_x$ contributes to the flipping of the TLS between its two eigenstates.[109,114] The flipping rate constants can be derived from Fermi's golden rule:[109]

$$\begin{aligned} k_{\mathrm{u}} &= cJ^2E\frac{1}{e^{\beta E} - 1} \\ k_{\mathrm{d}} &= cJ^2E\frac{1}{1 - e^{-\beta E}} \end{aligned} \tag{7}$$

Here k_{u} and k_{d} are the upward and downward transition rate constants, respectively, $\beta = 1/kT$, c is the TLS−phonon coupling constant, and we have used a density of acoustic modes quadratic in frequency in accord with the Debye model. The value of c can be independently evaluated from measurable acoustic properties of the glass by using the following relationship:[84,115]

$$c = \left(\frac{2\gamma_{\mathrm{t}}^2}{\upsilon_{\mathrm{t}}^5} + \frac{\gamma_{\mathrm{l}}^2}{\upsilon_{\mathrm{l}}^5}\right)\frac{1}{2\pi\rho_{\mathrm{m}}\hbar^4} \tag{8}$$

where $\gamma_{\mathrm{t}}(\gamma_{\mathrm{l}})$ and $\upsilon_{\mathrm{t}}(\upsilon_{\mathrm{l}})$ are the transverse (longitudinal) deformation potential parameter and velocity of sound, respectively, and ρ_{m} is the mass density of the glass. The parameters determining c in eq 8 are known for many glasses.[116] It is convenient to define the total flipping rate constant as the sum of the upward and downward rate constants:

$$K = k_{\mathrm{u}} + k_{\mathrm{d}} = cJ^2E\coth(\beta E/2) \tag{9}$$

The equilibrium, or equivalently, the time-averaged, occupation probablity of the excited state is

$$p = \frac{k_{\mathrm{u}}}{k_{\mathrm{u}} + k_{\mathrm{d}}} = \frac{1}{1 + e^{\beta E}} \tag{10}$$

The theoretical analysis in this paper is presented in terms of p and K, rather than k_{u} and k_{d}.

We next consider the question of which are the relevant TLS−TLS and TLS−chromophore coupling mechanisms (chromophore−chromophore coupling can be ruled out due to the chromophore's very low concentration). TLS−TLS and TLS−chromophore interactions are mediated by the strain field, or are electrostatic in origin. Resonant coupling, where two TLSs exchange energy by mutual excitation and deexcitation, is highly unfavorable in light of the wide distribution of TLS energies in a glass.[77] Similar resonant TLS−chromophore coupling can also be ruled out due to the huge mismatch between the electronic transition frequency of the chromophore and the much smaller energy splittings of the TLSs ($\sim kT$). On the other hand, nonresonant TLS−TLS and TLS−chromophore couplings must be included. In this case, the adjustment of the environment to a transition of one TLS gives rise to a strain field, which affects the energy levels of another TLS or of the chromophore itself. Such nonresonant TLS−TLS coupling is believed to be responsible for pure dephasing in the TLSs, which can be directly observed in phonon echo experiments.[77,85] However,

it is of lesser significance in the case of optical spectroscopy, where the dephasing of the chromophore (rather than that of the TLSs) is being directly measured. While it is true that a TLS flip will affect the energy splitting of a nearby TLS, as long as this perturbation is small compared to the energy splitting itself, the flipping rate of the affected TLS will hardly change. Thus, as far as the optical spectroscopy of the chromophore is concerned, we consider the TLSs to be independent. However, the nonresonant TLS−chromophore coupling is of central importance to the optical spectroscopy of the chromophore, since it is directly responsible for the chromophore's frequency fluctuations. In fact it is exactly this coupling that enables us to infer something about the glass dynamics from the chromophore's line shape.

One usually avoids a detailed treatment of the mechanism underlying the above strain-mediated nonresonant TLS−chromophore coupling. Instead, a stochastic approach is adopted, which is based on the sudden jump model of Klauder and Anderson.[77,88] Within this model, the excitation of the jth TLS instantaneously leads to a shift of the chromophore's transition (angular) frequency by υ_j. Thus, the chromophore's transition frequency at any given time is given by[4,93,95,102,103,117−121]

$$\omega(t) = \omega_0 + \sum_j \zeta_j(t)\upsilon_j \tag{11}$$

where $\zeta_j(t) = 0$ or 1 corresponds to the jth TLS being in its ground or excited state at time t, respectively, and ω_0 is the transition angular frequency when all the TLSs are in their ground states. It should be emphasized that each chromophore molecule feels a different static local field due to frozen disorder and therefore has a different ω_0. However, since all the experimental observables discussed below are independent of the frequency origin, ω_0 can be set to zero without loss of generality.

To predict the explicit form of υ_j would require a detailed understanding of the molecular motions underlying the glassy TLSs, which is currently unavailable (see however refs 106−108). It is known, however, that a local perturbation to the glass, such as a TLS flip, gives rise to a strain field that falls such as the inverse of the third power of the distance from the TLS. The TLS therefore behaves like an "elastic dipole moment".[77,93] Furthermore, a TLS−chromophore interaction of the dipolar type,[88,122,123] which falls such as the inverse of the third power of the TLS−chromophore distance, was found to be consistent with the results of numerous spectroscopic experiments. One consequently expects υ_j to involve an angular dependence originating from the orientation of the chromophore dipole relative to the "TLS dipole". Since this nonresonant TLS−chromophore interaction is mediated by a strain field, it also depends on how the TLS is coupled to this field. This coupling arises from the term linear in $\tilde{\mathbf{S}}_z$ in eq 6, which implies that υ_j is linear in A_j/E_j. Thus, υ_j is assumed to have the following form:

$$\upsilon_j = 2\pi\alpha\frac{A_j}{E_j}\frac{\epsilon_j}{r_j^3} \tag{12}$$

where α is the TLS−chromophore coupling constant, and A_j, E_j, ϵ_j, r_j are the asymmetry, energy splitting, orientation parameter, and distance relative to the chromophore, of the jth TLS, respectively.

The last component of the TLS model involves specifying the distribution of the TLS parameters r_j, ϵ_j, A_j, and J_j. We assume that the glass surrounding the chromophore behaves in much the same way as it would in its absence, i.e., that the TLS−chromophore coupling is weak. Hence, r_j and ϵ_j, which are properties defined relative to the chromophore, are taken to be independent of A_j and J_j, which are intrinsic properties of the neat glass. The present poor understanding of the angular dependence of υ_j justifies adopting the simplest model for ϵ_j, and thus we assume that $\epsilon_j = \pm 1$, with equal probability. Using a different (and more realistic) angular dependence would simply result in a renormalization of the TLS−chromophore coupling constant. Thus, ϵ_j is taken to be independent of r_j, with the following distribution:

$$P_\epsilon(\epsilon) = {}^1/_2[\delta(\epsilon - 1) + \delta(\epsilon + 1)] \tag{13}$$

The large typical average distance between thermally populated TLSs (∼10 nm) and the macroscopic homogeneity of glasses leads to the choice of a uniform distribution of the spatial locations of the TLSs:

$$P_r(r) = \begin{cases} \dfrac{3r^2}{r_{\max}^3} & \text{if } r < r_{\max} \\ 0 & \text{if } r > r_{\max} \end{cases} \tag{14}$$

The cutoff distance $r_{\max}$ is introduced in order to make the distribution normalizable. It must be large enough so that it does not affect the theoretical predictions.

The distribution of the TLS asymmetries A was assumed constant in early studies.[82,83] In order to justify this it was argued that the distribution function must be an even function of A, as positive and negative asymmetries are equally likely. Since it should also be continuous, it must have zero first derivative at $A = 0$. Therefore, on a scale of about 1 K, which is much smaller than the scale set by the glass transition temperature, the distribution is roughly constant.[70] However, the predictions regarding the temperature dependence of the heat capacity, heat conductivity, and chromophore spectroscopy are not entirely consistent with this distribution.[80] For example, the hole width in HB experiments typically varies as $T^{1.3}$ [124−126] rather than T, as predicted by the constant distribution hypothesis.[93,95,102] In order to resolve this discrepancy, one phenomenologically introduces an ad hoc distribution of A that goes such as A^μ, with μ a small fraction, typically around 0.3.[15,95,96,124−130] This yields hole widths whose temperature dependence is dominated by a $T^{1+\mu}$ power law, in accord with experiment. Although the behavior of this distribution function at $A \to 0$, where it goes to zero, is surely unrealistic, the main effect of this modification is to make the distribution rise slowly, rather than being a constant throughout most of the range of values of A. Thus, the distribution of asymmetries that is most consistent with experiment is

$$P_A(A) = \frac{1+\mu}{A_{\max}^{1+\mu}} \times \begin{cases} A^\mu & \text{if } 0 \le A < A_{\max} \\ 0 & \text{otherwise} \end{cases} \tag{15}$$

The cutoff $A_{\max}$ must be large enough so as not to affect the theoretical predictions. TLSs with $\beta E \gg 1$ have $p \ll 1$ (cf eq 10). Such TLSs are nearly always found in their ground states and, therefore, make no contribution to the fluctuating transition frequency of the chromophore. Thus, the cutoff of the TLS asymmetry should be set such that $A_{\max} \gg kT$.

The distribution of the TLS tunneling matrix element J is usually assumed to go like $1/J$. This results from the fact that for general double wells, $J \sim e^{-\lambda}$, where λ is a function of the barrier height and width, as well as of the effective mass, of the tunneling object. A broad distribution of λ is expected in glasses, which is usually assumed constant in the absence of any further information on its detailed form. This leads to the following distribution in J:

$$P_J(J) = \frac{1}{\ln(J_{max}/J_{min})} \times \begin{Bmatrix} J^{-1} & \text{for } J_{min} \le J \le J_{max} \\ 0 & 0 \text{ otherwise} \end{Bmatrix} \quad (16)$$

The upper cutoff J_{max} must be large enough so as not to affect the theoretical predictions. Similarly to A_{max} this implies that $J_{max} \gg kT$. J_{max} is often associated roughly with $\hbar$ times the angular frequency of oscillation in one of the wells. If the latter is much greater than kT, only a single level in each of the wells will be occupied, which is consistent with the TLS model.

The lower cutoff J_{min}, is also chosen so as not to affect the theoretical results. For a given temperature, the smallest possible flipping rate K_{min} is obtained when $E = J_{min}$ (cf eqs 4 and 9). Since $J_{min} \ll kT$ (for $T \sim 1$ K),[115] this leads to (cf eq 9 and note that $\coth(z) \approx 1/z$ at $z \ll 1$):

$$K_{min} = 2cJ^2_{min}kT \quad (17)$$

As long as K_{min} is much smaller than the inverse of the relevant experimental time scale, which in this case is the time it takes to measure the line shape of a single molecule (call this time τ_m), the value of the cutoff will not affect the results. Therefore we choose J_{min} such that $J_{min} \ll 1/\sqrt{2ckT\tau_m}$. It is important to note that there seems to be no physical reason to impose a lower cutoff on J. Hence, the divergence at $J_{min} \rightarrow 0$ of the distribution in eq 16 probably signals its breakdown for very slow TLSs, as was recently demonstrated experimentally by Maier et al.[131]

Recently, motivated by numerically generated distributions of tunneling states,[106−108,132] a $1/J^{1-\nu}$ distribution of J with $\nu \approx 0.00-0.25$ was suggested by Silbey, Koedijk, and Völker.[80] Using this model, they obtained good fits to PE experiments occurring on short time scales ($<10^{-2}$ s) by using $\nu \approx 0.15$. However, the best fit for HB experiments on longer time scales (10 s and longer) yields $\nu \approx 0$. Since the time scale of SMS line-shape measurements is similar to the latter, one does not expect to find significant improvement by introducing an extra parameter ν. Hence, the more traditional distribution in eq 16 is exclusively used in the present work.

This concludes our discussion of the standard tunneling model of low-temperature glasses and the sudden jump model, specialized for the case of optical spectroscopy of dilute chromophores. At first sight the model seems to depend on a large number of parameters. However, as indicated by the discussion above, all the cutoffs should not affect the final results if chosen properly. Naturally, this is only true if one adopts the point of view that nothing in the physics of glasses seems to impose true cutoffs. The remaining parameters are then the temperature T; the measuring time τ_m; the TLS−phonon coupling constant c, which is an intrinsic property of the neat glass and can be obtained from acoustic measurements; the power law of the asymmetry distribution μ, which can be estimated from the temperature dependence of spectral hole widths and echo decay rates; the TLS density ρ, which can be estimated from heat capacity measurements; and the TLS−chromophore coupling constant α, which is unknown, and will be treated as an adjustable parameter.

III. Line Shape of A Single Molecule

Let us now consider an individual chromophore, which is surrounded by many TLSs, whose locations, orientations, asymmetries, and tunneling matrix elements are randomly drawn from the distributions in eqs 13−16. The absorption line shape of such a single chromophore is given by the Fourier−Laplace transform of the dipole autocorrelation function:[118,133]

$$I(\omega) = Re\left(\frac{1}{\pi}\int_0^\infty dt\, e^{i\omega t}\, e^{-t/2T_1}\Phi_{SM}(t)\right) \quad (18)$$

where T_1 is the lifetime of the chromophore's excited state and

$$\Phi_{SM}(t) = \langle e^{-i\int_0^t d\tau\, \omega(\tau)}\rangle \quad (19)$$

$\omega(\tau)$ is the fluctuating frequency in eq 11, but with $\omega_0 = 0$. The average in eq 19 is over all stochastic realizations of the frequency trajectory $\omega(\tau)$ within the interval $(0, t)$. Further averaging over the locations, orientations, and internal parameters of the TLSs *is not performed*, since each individual chromophore only interacts with one distinct set of TLSs.

Since the flipping dynamics of each TLS is independent of that of the others, the average in eq 19 may be written as a product of single-TLS averages. Thus,

$$\Phi_{SM}(t) = \prod_j \phi_j(t) \quad (20)$$

where,

$$\phi_j(t) = \langle e^{-iv_j\int_0^t d\tau\, \xi_j(\tau)\Theta(K_j - \tau_m^{-1})}\rangle \quad (21)$$

and $\Theta(x)$ is a unit Heaviside function ($\Theta(x) = 1$ if $x > 0$, 0 otherwise). This Heaviside function is present since the dynamics of a TLS with $K < \tau_m^{-1}$ (recall that τ_m is the time it takes to measure a single-molecule line shape) will not contribute to the line shape. The average in eq 21 is now over all the stochastic realizations of $\xi(\tau)$ within the time interval $(0, t)$. This average can be evaluated exactly using the techniques developed by Anderson[134] and Kubo,[135] leading to[118,121]

$$\phi_j(t) = \begin{Bmatrix} e^{-1/2(K_j + iv_j)t}\,[\cosh(\Omega_j t) + \alpha_j/\Omega_j \sinh(\Omega_j t)] & \text{if } K_j \ge \tau_m^{-1} \\ 1 & \text{if } K_j < \tau_m^{-1} \end{Bmatrix} \quad (22)$$

where

$$\Omega_j = \sqrt{\frac{K_j^2}{4} - \frac{v_j^2}{4} - i\left(p_j - \frac{1}{2}\right)v_j K_j} \quad (23)$$

and

$$\alpha_j = \frac{K_j}{2} - i(p_j - {}^1/_2)v_j \quad (24)$$

Substituting eq 22 into eq 20 and substituting the result into eq 18 yields the single-molecule line shape for a given TLS environment. The evaluation of the integral in eq 18 is carried out numerically. The resulting line shape is generally not Lorentzian, nor does it assume any other simple form.

Considering the relative complexity of the single-molecule line shape formula, it is rather surprising that its average over all possible TLS environments turns out to be a simple Lorentzian! We leave the details of the derivation to Appendix A. The final result is

$$\langle I(\omega)\rangle = \frac{\gamma/\pi}{\omega^2 + \gamma^2} \quad (25)$$

where $\langle I(\omega)\rangle$ is the average SMS line shape and

$$\gamma = \frac{1}{2T_1} + \frac{2\pi^3}{3}\alpha\rho P_0 (kT)^{1+\mu}\int_0^\infty dz \frac{z^\mu}{1 + e^z} \times$$

$$\int_0^{\Gamma_m z^3 \coth(z/2)} \frac{dx}{x}\left(1 - \frac{x}{\Gamma_m z^3 \coth(z/2)}\right)^{\mu/2}\Theta(x-1) \quad (26)$$

where

$$P_0 = \frac{1+\mu}{A_{max}^{1+\mu}\ln(J_{max}/J_{min})} \quad (27)$$

ρ is the TLS density, and $\Gamma_m = c(kT)^3\,\tau_m$. It should be emphasized that this is the average of the single-molecule line shapes, each shifted to the same frequency origin, i.e., having the same $\omega_0 = 0$. In the experiment, different chromophores have different values of ω_0 due to inhomogeneous broadening. Since these different frequency origins are unknown (they do not in general correspond to the peaks of the single-molecule line shapes), one cannot shift all experimental line shapes to the same frequency origin in the above sense. As a result, one cannot compare the average in eq 25 to experiment. Nonetheless, it will be interesting to compare the width of the average single-molecule line shape to other "line widths", as determined by PE and HB experiments.

IV. Photon Echo and Hole-Burning Spectroscopies

One of the goals of this work is to analyze SMS, PE, and HB experiments, all within the same theoretical model. To this end, we need to discuss theoretical results for the PE and HB intensities. It has recently been shown that all experimental PE and HB observables are related to the three-pulse photon echo (3PE) amplitude.[94,101,102] In the 3PE experiment the sample is subjected to three $\pi/2$ pulses. The first two pulses are separated by a time τ, the second and third pulses are separated by a time T_w, and the echo appears at a time τ after the third pulse. The 3PE amplitude is given by[15,77,88,94,101,102]

$$P(\tau, T_w) = e^{-\tau/T_1}\langle e^{-i[\int_0^{\tau} dt\,\omega(t) - \int_{T_w+\tau}^{T_w+2\tau} dt\,\omega(t)]}\rangle \quad (28)$$

where $\omega(t)$ is defined as in eq 11 but with ω_0 set to zero. The average in eq 28 is over the locations, orientations, and internal parameters of the TLSs and, also, over the stochastic realizations of the frequency trajectory within $(0, T_w + 2\tau)$. The typical 3PE experiment involves the measurement of the echo intensity at a time $T_w + 2\tau$, which is proportional to $I(\tau, T_w) = |P(\tau, T_w)|^2$, as a function of τ for a given waiting time T_w. It is also known that the hole shape in a HB experiment is proportional to the Fourier transform of $P(\tau, T_w)$ with respect to τ. In this case T_w is interpreted as the time between burning and reading.[94,102] The amplitude for the two-pulse echo (2PE) experiment can be obtained from the above by setting $T_w = 0$. Thus the 2PE intensity is proportional to $I(\tau, 0) = |P(\tau, 0)|^2$.[77,88,94,102]

Hu and Walker showed how to perform the averages in eq 28 over the spatial and orientational distributions for the TLSs (see eqs 13 and 14) and over the stochastic time histories.[136] Their procedure gives[105]

$$P(\tau, T_w) = e^{-\tau/T_1}e^{-F(\tau)}e^{-G(\tau,T_w)} \quad (29)$$

where

$$F(\tau) = \frac{2\pi^3}{3}\alpha\rho\left\langle\frac{A}{EK}\,\mathrm{sech}^2(\beta E/2)F(\tanh(\beta E/2), K\tau)\right\rangle \quad (30)$$

$$G(\tau, T_w) = \frac{2\pi^3}{3}\alpha\rho\left\langle\frac{A}{EK}\,\mathrm{sech}^2(\beta E/2)G(\tanh(\beta E/2), K\tau)(1 - e^{-KT_w})\right\rangle \quad (31)$$

In the above

$$F(\xi, x) = 2e^{-x}\int_0^x dx' I_0[\xi(x-x')]x'[I_0(x') + I_1(x')] \quad (32)$$

$$G(\xi, x) = \frac{1}{2}\frac{\partial F(\xi, x)}{\partial x} = e^{-x}\int_0^x dx' I_0[\xi(x-x')]I_0(x') \quad (33)$$

and $I_0(z)$ and $I_1(z)$ are the modified Bessel functions of the first kind of order 0 and 1, respectively.[137] The averages in eqs 30 and 31 are now over only the distributions of A and J (see eqs 15 and 16).

The approximate evaluation of the integrals implicit in these averages has been discussed by many, and there seem to be generally accepted procedures for both $F(\tau)$[80,91,97,99,101,102] and for $G(\tau, T_w)$.[77,80,93,138] The results of these analyses show that both $F(\tau)$ and $G(\tau, T_w)$ are approximately linear in τ. Defining $F(\tau) = 2\tau/T_2'$, and $G(\tau, T_w) = 2\tau/T_2^{SD}$, one has[105]

$$\frac{1}{T_2'} = \frac{\pi^3}{6}\alpha P_0\rho(kT)^{1+\mu}\,B(\mu) \quad (34)$$

$$\frac{1}{T_2^{SD}} = \frac{\pi^3}{6}\alpha P_0\rho(kT)^{1+\mu}[C(\mu)\ln[c(kT)^3T_w] + D(\mu)] \quad (35)$$

where $B(\mu)$, $C(\mu)$, and $D(\mu)$ are dimensionless functions of μ; specific values are:[105] $B(0) = 7.327\,72$, $B(^1/_3) = 7.880\,61$, $C(0) = 2$, $C(^1/_3) = 2.042\,25$, $D(0) = 2.401$, and $D(^1/_3) = 4.012$. Within these approximations the total 3PE amplitude therefore decays exponentially, as $P(\tau, T_w) = e^{-2\tau/T_2(T_w)}$, where $1/T_2(T_w) = 1/2T_1 + 1/T_2' + 1/T_2^{SD}$, and the hole half-width in a HB experiment is $\Delta\nu/2 = 1/\pi T_2(T_w)$. Note that, in the 2PE experiment, $T_w = 0$, $1/T_2^{SD} = 0$, and $1/T_2 \equiv 1/T_2(0) = 1/2T_1 + 1/T_2'$.

In a recent paper, however, we have shown that these approximate results are not quantitatively accurate for parameters appropriate for systems that have been studied experimentally.[105] Therefore, for the comparisons about to be undertaken, we prefer to use the exact results that emanate from the Hu−Walker equations. For the distributions of A and J discussed in the present paper, these are[105]

$$F(\tau) = \frac{\pi^3}{3}\alpha P_0\rho(kT)^{1+\mu}\tau\int_0^{\infty} dz\, z^{\mu}\,\mathrm{sech}^2(z/2)\int_0^{\Gamma z^3\coth(z/2)}\frac{dx}{x^2}\times\left(1 - \frac{x}{\Gamma z^3\coth(z/2)}\right)^{\mu/2}F(\tanh(z/2), x) \quad (36)$$

$$G(\tau, T_w) = \frac{\pi^3}{3}\alpha P_0\rho(kT)^{1+\mu}\tau\int_0^{\infty} dz\, z^{\mu}\,\mathrm{sech}^2(z/2)\int_0^{\Gamma z^3\coth(z/2)}\frac{dx}{x^2}\left(1 - \frac{x}{\Gamma z^3\coth(z/2)}\right)^{\mu/2}\times G(\tanh(z/2), x)(1 - e^{-T_w x/\tau}) \quad (37)$$

where $\Gamma = c(kT)^3\,\tau$.

One of the features of the exact results is that $F(\tau)$ and $G(\tau, T_w)$ are not generally linear in τ, although the deviations are slight.[105] Nonetheless, this makes it awkward to assign a single echo decay time. If these functions were linear in τ, as in the "standard" approximations described above, the 3PE intensity would decay exponentially: $I(\tau, T_w) = e^{-4\tau/T_2(T_w)}$. Thus we see that when $\tau = T_2(T_w)/4$ the intensity drops to 1/e of its initial value. More generally, for nonexponential decays we will define $T_2(T_w)$ by $I(T_2(T_w)/4, T_w) = 1/e$. Since the 2PE decay time is defined by $T_2 = T_2(0)$, this can be obtained from the above

TABLE 1: Experimental Conditions under Which Line-Width Distributions Were Measured

system	T (K)	τ_m (s)	no. of chromophores	ref
Tr/PE	1.8	200	176	64
Tr/PS	1.7	120	121	58
Tr/PMMA	1.7	120	68	58
Tr/PVB	1.7	120	211	58
TBT/PIB	1.4	2	173	59, 60
TBT/PE	1.4	2	113	59, 60

definition by simply setting $T_w = 0$. Finally, the hole shape in a HB experiment is given by[94,102]

$$I_{HB}(\omega, T_w) = Re\left(\frac{1}{\pi}\int_0^\infty d\tau\, e^{i\omega\tau} P(\tau, T_w)\right) \qquad (38)$$

We will characterize the (generally non-Lorentzian) hole shape by its fwhm.

V. Calculation of Line-Width Distributions and Comparison To Experiment

Distributions of single-molecule line widths in low-temperature glasses have been measured by Fleury et al. for terrylene (Tr) in polyethylene (PE);[64] by Kozankiewicz et al. for Tr in polystyrene (PS), poly(methyl methacrylate) (PMMA), and polyvinylbutyral (PVB);[58] and by Kettner et al. for tetra-*tert*-butylterrylene (TBT) in PE and polyisobutylene (PIB).[59,60] The distributions were measured at different temperatures, for various measuring times, and on different numbers of chromophores, as indicated in Table 1.

The theoretical approach that we use to calculate line-width distributions is as follows. In eqs 18, 20, and 22 we have presented an essentially exact (within the TLS and sudden jump models) formula for the calculation of the line shape of a single molecule interacting with a number of TLSs. We emphasize that for this calculation one must specify a specific set of parameters (ϵ, r, A, J) for each TLS. From the numerically calculated line shape, we can determine the line width (see below). To calculate the distribution of line widths we must then repeat this procedure many times, choosing the TLS parameters from the distributions specified earlier. Therefore the calculation of the line-width distribution involves a Monte Carlo simulation. To perform this simulation, we first need to discuss the parameters of the model, which are T, τ_m, T_1, c, μ, A_{max}, J_{max}, J_{min}, ρ, r_{max}, and α.

The temperature T and the measuring time τ_m are set by the experimental conditions (cf Table 1). The excited-state lifetime T_1 of Tr is known from experiments on the system Tr/PE to be $T_1 = 3.8$ ns.[49] In fact, T_1 of Tr may vary from host to host, and even from molecule to molecule in the same host, since the transition dipole of each chromophore depends on its microscopic environment. But we have no experimental information on these possible variations, so we simply take T_1 to be 3.8 ns for Tr in all hosts, for all molecules. Moreover, since TBT is a derivative of Tr and is believed to be solvated in a similar manner, we expect it to have a similar T_1, and we take it to be the same.

The TLS−phonon coupling constant c can be obtained from acoustic measurements (cf eq 8 and refs 84, 115, 116). Among the glasses under discussion, values of c are only known for PS ($ck^3 = 3.87 \times 10^8$ K^{-3} s^{-1}) and PMMA ($ck^3 = 1.16 \times 10^9$ K^{-3} s^{-1}).[116] To avoid a proliferation of adjustable parameters, for PE, PIB, and PVB we (somewhat arbitrarily) choose the value for PMMA. In any case, our results are only weakly (logarithmically) dependent on the value of c. For μ we choose $\mu = 1/3$. This choice is motivated by the experimental fact that hole widths generally increase with temperature like $T^{1.3}$.[124−130] Assuming that the hole widths are dominated by spectral diffusion, eq 37 implies that the hole width goes roughly like $T^{1+\mu}$ (but see also ref 105). This leads to the choice of $\mu = 0.3$. This is the same as $\mu = 1/3$, within experimental error, and the latter choice turns out to be convenient for evaluating the TLS density.

As discussed earlier, if we choose A_{max} and J_{max} to be much larger than kT, the results will not be sensitive to the values of the cutoffs. On the other hand, if we choose these cutoffs to be too large, then we waste computer time by simulating TLSs that are never thermally populated and therefore never contribute to the line shapes. Therefore we choose $A_{max}/k = J_{max}/k = 17$ K, which is about 10 times larger than T. Similar considerations apply to J_{min}. As long as J_{min} is much less than $(2ckT\tau_m)^{-1/2}$, the results will not be sensitive to this cutoff. For the systems studied herein, the latter quantity is between 2.5×10^{-5} kK and 2.5×10^{-6} kK, and so we choose $J_{min}/k = 2.76 \times 10^{-7}$ K, which is about 10 times smaller than the smallest of these values.

One finds values in the literature for the TLS spectral density (i.e., number of TLS per unit volume per unit energy) $n_s(E)$, evaluated from heat capacity[74] and acoustical measurements[116] that deviate by more than an order of magnitude for the same material. The value we take is from ref 74, which is the same for both PS and PMMA. In fact, the value quoted is actually the integral of $n_s(E)$ from $E = 0.5-1.5$ kK. From this we can calculate the total TLS density ρ. The details are described in Appendix B, and the result is $\rho = 1.15 \times 10^{-2}$ nm^{-3}. This corresponds to a typical distance between TLSs of about 4.4 nm. Note, however, that the TLS density ρ includes those TLSs with energy splittings up $E_{max} = \sqrt{A_{max}^2 + J_{max}^2} \simeq 24$ kK for our parameters and that many of these TLSs do not have appreciable thermal population at 1.7 K and therefore do not appreciably contribute to the line shapes. The density of thermally populated TLSs is about an order of magnitude smaller than that quoted above, and the typical distance between thermally populated TLSs is closer to 10 nm.

The value of the upper cutoff r_{max}, for the TLS−chromophore distance is chosen so that the perturbation to the chromophore's frequency from a TLS this distance away is much smaller than the perturbation from a typical nearby TLS. This leads to the condition that $\rho r_{max}^3 \gg 1$. In addition, we checked that increasing the value of r_{max} did not affect our results. Typically, we used $r_{max} \approx 30$ nm, so that each chromophore interacts with about 1000 TLSs, or with about 100 thermally populated TLSs.

To simulate the distribution of single-molecule line widths, the following scheme is implemented. For a given chromophore, the values of ϵ, r, A, and J for each TLS with which it is interacting are randomly chosen from the underlying distributions (cf eqs 13−16). With these values, $\Phi_{SM}(t)$ is evaluated (cf eqs 20 and 22), and then numerically Fourier transformed to obtain a single-molecule line shape. The line width is then determined by the fwhm of this line shape. More specifically, we find the absolute maximum of the line shape and then search outward on both sides until half the maximum is reached. This is repeated for a total of 2000 chromophores, and the resulting line width distribution is then presented as a histogram using the same bin width as in the corresponding experiments. Since all the parameters are fixed except for the TLS−chromophore coupling constant α, we use the latter as a fitting parameter. The simulated histogram is compared to the experimental one in a least-squares sense, and the entire procedure is repeated for different values of α.

Before we present the line width distributions, let us discuss several aspects of the simulations, for example, for Tr/PS. The single-molecule line shapes in this system are typically 1−2 orders of magnitude wider than the natural line width ($1/2\,\pi T_1$).

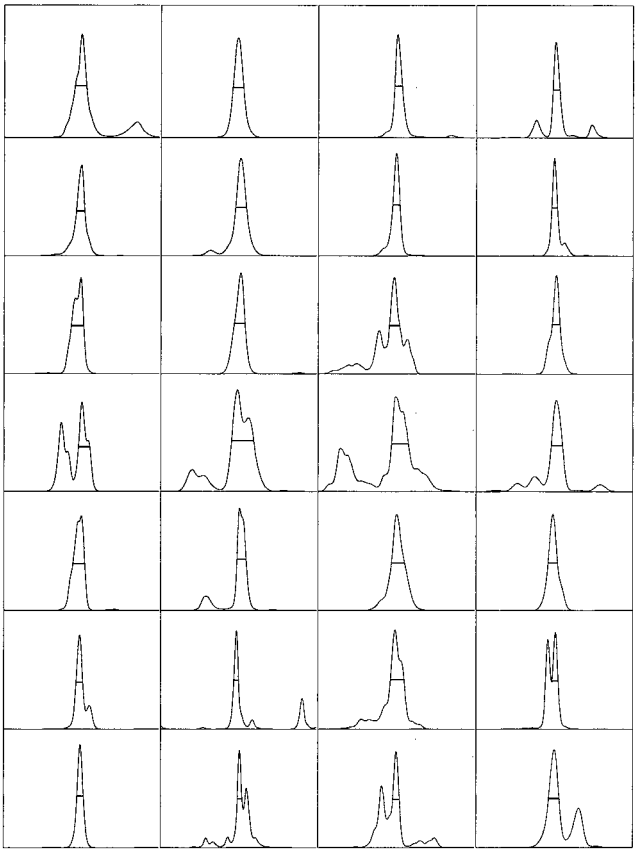

Figure 2. Randomly chosen simulated single-molecule line shapes (28) for Tr/PS. The *x* axis corresponds to a frequency range of 34 GHz. The scale along the *y* axis is not the same for different line shapes. The fwhm of each line line shape is indicated by a horizontal line.

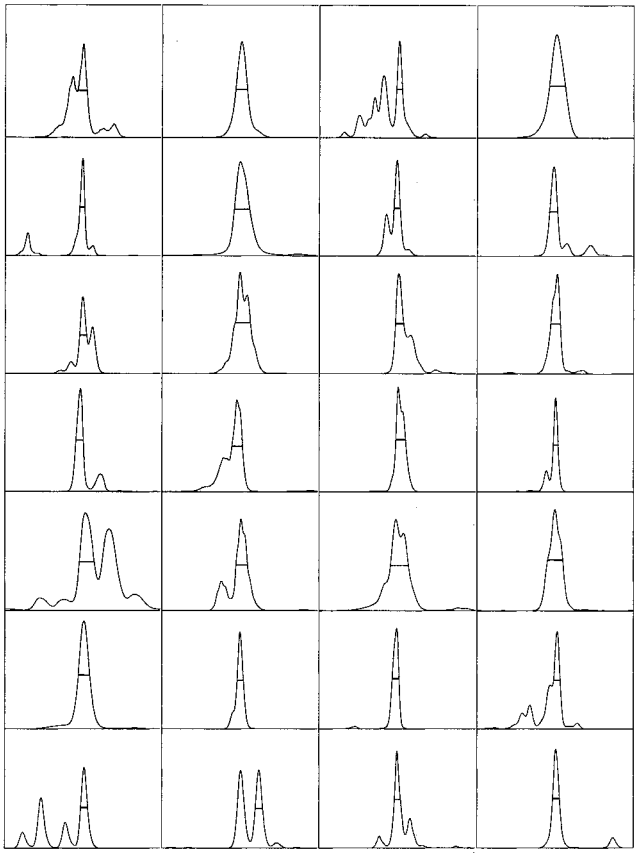

Figure 3. Randomly chosen simulated single-molecule line shapes (28) for Tr/PS. The *x* axis corresponds to a frequency range of 34 GHz. The scale along the *y* axis is not the same for different line shapes. The fwhm of each line line shape is indicated by a horizontal line.

One therefore expects pronounced signatures of TLS-induced broadening in this system. A set of 56 randomly chosen simulated Tr/PS single-molecule line shapes for $\alpha = 375$ GHz nm^3 (the value that leads to the best fit of the experimental distribution) are shown in Figures 2 and 3. One sees that the variety of possible line shapes is truly stunning! Each molecule has its own distinct line shape, showing unequivocally, at least for this model, that there really is no such thing as a "homogeneous line shape" for chromophores in glasses. We must emphasize that all of the stucture that is found in these line shapes arises from interactions with TLSs. In particular, a nearby TLS will produce a large perturbation, v, to the chromophore's transition frequency. It is likely that such a TLS will be in the "slow exchange" limit ($v > K$). If v is sufficiently large, the interaction with this TLS will produce a splitting of the line, corresponding to the two possible configurations of the TLS. The residual broadening of each component of the doublet arises from the chromophore's interaction with the remaining TLSs and from lifetime broadening. Two nearby TLSs will produce a quartet, etc. Therefore, within this model, one can understand, from the relatively strong distance dependence of the chromophore-TLS coupling and from the wide distributions of TLS−chromophore distances and TLS internal parameters, that a rich variety of single-molecule line shapes arises. It is important to point out that the experimental SMS line shapes are not as structured as our simulated line shapes. However, the signal-to-noise ratio in the experimental line shapes is quite low, and we believe that this noise could wash out much of the underlying structure

The diversity of simulated line shapes makes it hard to come up with an unambiguous definition of a *line width*. To check the sensitivity of the line-width distribution with respect to the line-width definition, we also evaluated the width in another way, namely by searching for the half-maximum points starting from both sides of the frequency range inward, rather than from the peak frequency outward. This newly defined width is always larger than or equal to the previous definition. If the latter underestimates the width in some cases, the former overestimates it. We found that the two widths coincide for 84−91% of the line shapes. Obviously, the line-width distributions based on the different definitions are somewhat different. As expected, the value of α that best fits the experimental distribution is slightly lower for the newly defined width. For example, using the new definition in the case of Tr/PS yields the best fit with $\alpha = 350$ GHz nm^3 rather than $\alpha = 375$ GHz nm^3, and the fit itself is slightly better. However, the statistical uncertainty due to the small size of the experimental sample makes this difference insignificant. Thus, at least for the experimental data available at present, the quality of the best fit and the corresponding value of α are essentially insensitive to the line-width definition. Of all the systems studied, the value of α turns out to be largest for Tr/PS. For smaller values of α, when the lifetime makes a larger relative contribution to the line shape, our definition becomes less ambiguous.

As a consistency check we calculate the average of the 2000 simulated line shapes, and we compare that to the theoretical average line shape for the same model predicted from eqs 25 and 26. The comparison is presented in Figure 4 for the case of Tr/PS with $\alpha = 375$ GHz nm^3. The excellent agreement between simulation and theory means that a sample of 2000 chromophores is already converged to a large extent. The fwhm of the average line shape, in hertz, is given by γ/π (see eq 26), which for Tr/PS is 1.76 GHz.

Once we have determined the best fit value of α from comparing the simulated and experimental line-width distributions, we can then go on to calculate the two-pulse echo decay

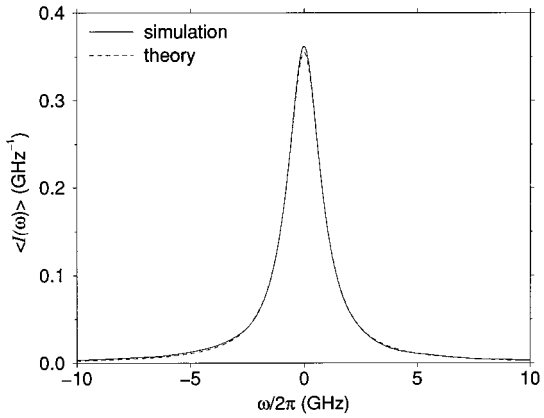

Figure 4. A comparison of the average of 2000 simulated line shapes (solid line) with the corresponding theoretical prediction, eqs 25 and 26 (dashed line). These line shapes correspond to the system Tr/PS with $\alpha = 375$ GHz nm^3.

TABLE 2: Best-Fit Values of α (in GHz nm^3) and Several Calculated "Line Widths" (All in MHz) for the Six Systems Studied

system	α	$1/2\pi T_1$	$1/\pi T_2$	$\Delta\nu_{HB}/2$	γ/π	$\langle\Delta\nu\rangle$
Tr/PS	375	42	135	1444	1794	1966
Tr/PMMA	190	42	108	778	981	1092
Tr/PVB	120	42	85	499	629	684
Tr/PE	12	42	47	91	107	117
TBT/PIB	25	42	49	100	118	127
TBT/PE	30	42	50	112	133	144

TABLE 3: Calculated and Experimental Echo Decay Rates and Hole Half-Widths (All in MHz) for the Six Systems Studied

system	$1/\pi T_2$	$1/\pi T_2$ (standard)	$1/\pi T_2$ (exptl)	$\Delta\nu_{HB}/2$	$\Delta\nu_{HB}/2$ (standard)	$\Delta\nu_{HB}/2$ (exptl)
Tr/PS	135	235		1444	1647	1600[58]
Tr/PMMA	108	142		778	902	900[58]
Tr/PVB	85	104		499	579	550[58]
Tr/PE	47	48		91	101	
TBT/PIB	49	51	106[139,140]	100	114	180[140]
TBT/PE	50	53	83[141]	112	128	

time T_2 and the hole width $\Delta\nu_{HB}$ with no adjustable parameters, using the formulas and procedures described in section IV. To compare the latter quantity with our single molecule results, we will take $T_w = \tau_m$. That is, we assume that the waiting time in the hole burning experiments is the same as the measuring time in the single molecule experiments. In fact, experimentally, these two times are on the same order of magnitude, and in any case, the sensitivity of either the single molecule or hole burning results is logarithmic in this time. In Table 2 we compare, for Tr/PS, $1/2\pi T_1$, $1/\pi T_2$, $\Delta\nu_{HB}/2$, γ/π, and $\langle\Delta\nu\rangle$ (the average single-molecule line width). Note that, if there were a "homogeneous line shape", and such a line shape were Lorentzian, these last three quantities would all be the same. But there is no homogeneous line shape in these systems, and in fact, these three quantities are all different. This makes sense—in general, there is no reason to expect the width of the average line shape to equal the average single-molecule line width. In addition, the theoretical results for the width of the average line shape and for the hole width are different mathematical expressions, which, again, should give different results.

For Tr/PS we can compare our calculated (using no adjustable parameters) hole half-width $\Delta\nu_{HB}/2 = 1.444$ GHz with the experimental value of $\Delta\nu_{HB}/2 = 1.600$ GHz[58] (see Table 3). These two values, though not identical, agree to within 10%. Also shown in Table 3 is the comparison of the "standard" approximations to the hole width, from eqs 34 and 35, to our exact calculation, and the "standard" approximation (from eq 34) and exact results for the 2PE decay time T_2. One sees that these two calculated hole widths differ by about 15%, but that the two calculations for T_2 differ by nearly a factor of 2. We do not know of any 2PE experiments on the system Tr/PS.

Finally, we compare the simulated and experimental single-molecule line-width distributions for Tr/PS in Figure 5. As described earlier, this calculation involves one adjustable parameter, the TLS−chromophore coupling constant α. From the figure one sees, first of all, that the simulated histogram is much smoother than the experimental one. This is simply due to statistical fluctuations arising from the smaller experimental (121 chromophores) than simulated (2000 chromophores) data sets. The shapes of the simulated and experimental distributions are very similar, with a sharp leading edge for small line widths and a gradual falling edge for large line widths. Apart from the experimental peak in the distribution just above 2 GHz, which we think is a statistical fluctuation (see some of the other plots in Figure 5), the major difference between the simulated and experimental distributions occurs for small values of the line widths, where the experimental distribution is larger than the simulated one. To see whether this deviation can be accounted for by statistical fluctuations, we ran several simulations with exactly the same number of chromophores as were studied experimentally. On the basis of these simulations we conclude that these deviations are statistically significant and cannot be accounted for by statistical fluctuations.

We now go on to discuss the other five systems studied experimentally. Using the values of α obtained from fitting the line-width distributions, the calculated values of the single molecule and "ensemble" (echo and hole burning) observables are shown in Table 2. In all cases the results are qualitatively similar: the 2PE "line width" is larger than the lifetime-limited line width because of "pure dephasing"; the hole half-width is larger still because of "spectral diffusion"; and the hole half-width, the width of the average single-molecule line shape, and the average of the single-molecule line widths are all different. In Table 3 one sees that the experimental hole widths for Tr/PMMA and Tr/PUB are in reasonable agreement with theory. For TBT/PIB T_2 and the hole width have been measured,[139,140] and T_2 has also been measured for TBT/PE.[141] As seen from Table 3, these experimental results are substantially larger than our theoretical predictions. The reason for these discrepancies is not clear. For the echo experiments, one possibility involves the fact that the echo samples are much higher in chromophore concentration than the SMS samples. In the former case, chromophore−chromophore interactions can lead to enhanced 2PE decay rates.

In Figure 5 are shown the single-molecule line-width histograms, both simulated and experimental, for the other five systems. In all cases, the qualitative agreement between simulation and experiment is good, but in all cases the simulations predict somewhat too few molecules with narrow line widths.

One possible origin of the discrepancies between simulated and experimental line-width distributions involves the experimental noise in the measurement of the single-molecule line shapes, which is considerable. Another involves the differences in the experimental and simulation determinations of the single-molecule line widths. Experimentally, the line shapes were fit to Lorentzians, and the widths were determined from these fits, while in the simulation line widths were taken from the fwhms, as described above, of the simulated line shapes. Our best guess, however, is that neither of these possibilities can account for the observed discrepancies.

Another possibility involves the uncertainty in some of the parameters we have chosen. In particular, the value of ρ is

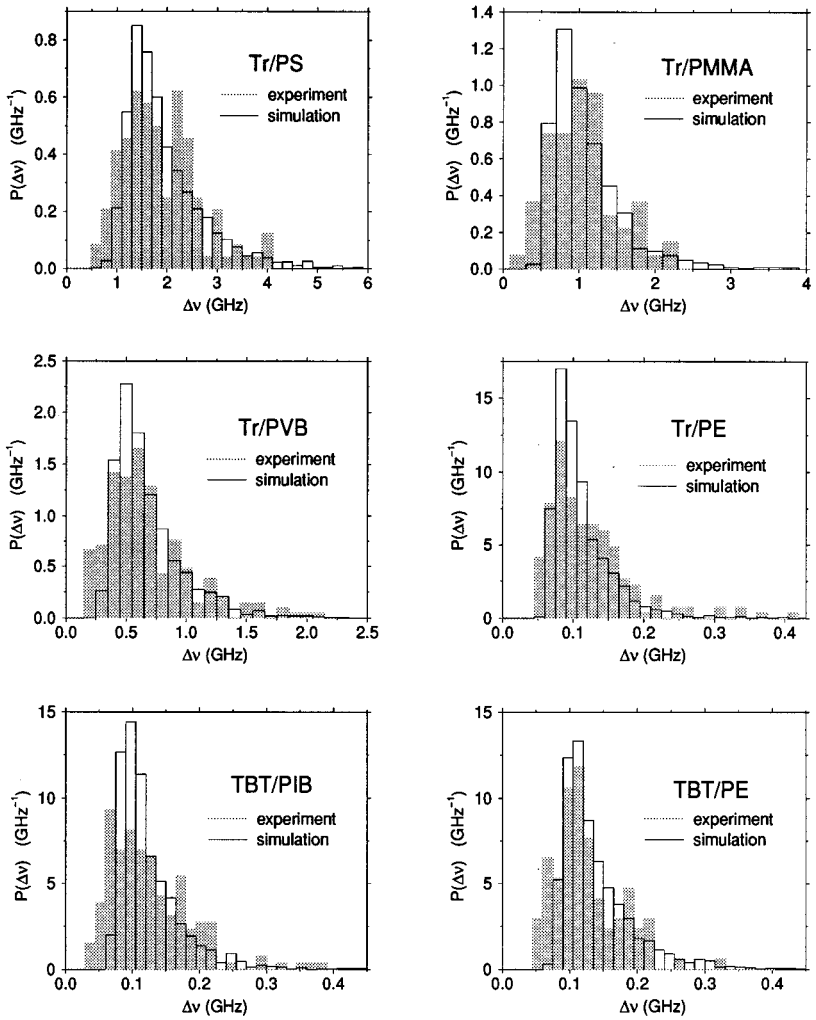

Figure 5. Single-molecule line-width distributions for Tr/PS, Tr/PMMA, Tr/PVB, Tr/PE, TBT/PIB, and TBT/PE (cf. Table 1), simulation vs experiment. All simulated distributions correspond to samples of 2000 chromophores.

uncertain, even in polymers for which it has been explicitly measured, and the simulation results depend dramatically on ρ. However, one can show that the simulation results actually only depend on the product $\alpha P_0 \rho$, and α is treated as an adjustable parameter. This means that any errors introduced by an incorrect value of ρ will be compensated for by the best-fit value of α. The value of c is known for only two polymers, and one of these values was used for the other polymers. However, the simulation and theoretical results seem to depend only logarithmically on c, and so this is not likely to be the source of the discrepancies. The correct value of μ is also uncertain, because of the range of reported temperature exponents obtained from hole burning experiments and because of the ambiguities of associating those temperature exponents with μ.[105] We have performed a few calculations for Tr/PS for $\mu = 0$, obtaining results similar to those for $\mu = {}^1/_3$. More work along these lines should probably be done. We have assumed the same value of T_1 for all chromophores and hosts, which is probably an oversimplification. For example, the fluorescence lifetime of the chromophore resorufin is known to vary from one host to another,[94] and also may well vary from molecule to molecule in the same host. Of course, any error associated with inaccuracies in T_1 will not be important in those cases where the line shapes are dominated by TLS dynamics.

Finally, it is possible that the source for the discrepancy lies in the standard tunneling TLS model itself. That is to say, some of our choices for the distributions could be in error. For example, perhaps the spatial distribution of TLSs is not isotropic, and that the chromophore somehow excludes TLSs from its nearby vicinity. This could account for the greater preponderance of narrow line widths in experiment than in simulation. In addition, perhaps there is a distribution of TLS−chromophore coupling constants, and this distribution is correlated with other distributions, for example, with the distribution of tunneling matrix elements (or flip rates).[142] Perhaps the one-phonon-assisted tunneling model is not appropriate for all TLSs; flipping of some TLSs might, for example, involve a two-phonon Raman process.[64]

Before leaving this section we note that Fleury et al.[64] have previously performed a related theoretical analysis of SMS line width distributions. They assumed that all TLSs are in the "slow-exchange" limit, and they then characterized each line shape by its second moment.[121] These simplifications lead to an analytic theory of line width distributions, whose shape does indeed resemble the experimental ones. However, comparison to our numerical calculations, for the same model and parameters, shows that this analytic distribution is not quantitatively accurate.

VI. Concluding Remarks

The standard TLS model, combined with the assumptions of one-phonon-assisted tunneling, as well as dipolar TLS−chromophore interactions, has been used for over a decade to describe photon echo and hole burning experiments on chromophores in low-temperature glasses. We have shown that from the same model naturally arises a fascinating distribution of single-molecule line shapes. With a single adjustable parameter

we have compared our theoretical single-molecule line-width distributions with those measured experimentally, finding reasonably good agreement. In addition, with no adjustable parameters, we have then calculated echo decay rates and hole widths for the same systems, and our results are in reasonable agreement with some, but not all, experiments. Inasmuch as single molecule experiments provide a discriminating test of the TLS model, because they measure distributions rather than averages of dynamical behavior, these results provide evidence that the standard TLS model is basically correct. On the other hand, there are systematic discrepancies between the simulated and experimental single-molecule line-width distributions and between the theoretical and experimental hole widths and echo decay rates. At this point we do not know whether the origin of these discrepancies lies in oversimplifications inherent in the standard TLS model, or results from less fundamental issues.

To resolve this question we need more single molecule experiments. In particular, distributions of single-molecule line widths have inherent statistical noise, and the more line widths one can measure, the smaller are these statistical fluctuations. Measuring 500 or 1000 line shapes for the same system at the same temperature would probably be sufficient. And of course, the smaller the signal-to-noise on each line shape the better! One also probably needs to characterize these line shapes more accurately than by fitting to Lorentzians. The temperature dependence of these line-width distributions is another fruitful and unexplored avenue. Even more interesting is the distribution of single-molecule temperature dependences. That is, since each molecule has its own TLS environment, it should have a unique temperature dependence to its line shape. Finally, single-molecule experiments will be most revealing when combined with other ensemble experiments on the same systems, such as three-pulse echoes and hole burning. These experiments have a dynamic range that cannot be matched (at present) by single molecule experiments, and as such they provide complementary information.

Our understanding of the optical spectroscopy of chromophores in condensed phases has evolved gradually over the years. Seventy years ago we understood that the chromophore's excited-state lifetime caused a broadening of the absorption line shape. Forty years ago we understood that dynamical fluctuations of the chromophore's transition frequency, called pure dephasing, produced an additional breadth of the line. It was generally understood that these fluctuations were the same for each chromophore—hence the term homogeneous line shape. It was also understood that different molecules had different static transition frequencies, and that this distribution caused inhomogeneous broadening. Thirty years ago it was discovered that this inhomogeneous broadening could magically be removed by line-narrowing techniques, revealing the homogeneous line shape. Only 10 years ago further experiments showed that in fact this homogeneous line shape depended on the time scale of the experiment, because of slow fluctuations called spectral diffusion. And then 5 years ago some of the first single molecule experiments in glasses showed that, in fact, each chromophore has a different line shape, demonstrating directly that the concept of a homogeneous line shape is not correct (for these systems) and further implying that the dynamical fluctuations felt by each chromophore are different.

In retrospect, this latter finding makes perfect sense. We have known for years[6] that a point chromophore interacting in a dipolar manner with a collection of point perturbers leads to a Lorentzian inhomogeneous line shape. That is, each chromophore has a different environment, due to the particular set of perturbers with which it is interacting. The standard TLS model of chromophores in glasses discussed herein is nothing more than a dynamic version of this model. That is, now the chromophore is interacting with a set of point perturbers with internal dynamics. So we should not be surprised that each chromophore experiences different dynamical fluctuations.

Nonetheless, we did not anticipate this fact, because we did not think about what individual molecules might be doing, because we did not think we would ever have the luxury of measuring them. The evolution of our understanding of chromophore spectroscopy in glasses illustrates the power of "getting inside the ensemble average", in this case by measuring the properties of individual molecules. Very generally, it is our belief that, more and more, as we are able to study individual members of an ensemble, we will find distributions of behavior, and that these distributions will bring new understanding.

Acknowledgment. We thank Michel Orrit, Boleslaw Kozankiewicz, Ross Brown, Urs Wild, Bob Silbey, Michael Fayer, Thomas Basché, Stephan Zilker, Boris Kharlamov, and Frank Brown for helpful discussions. E.G. is grateful for Fellowships from the Fulbright Foundation and the Hebrew University. J.L.S. acknowledges support from the National Science Foundation (Grants CHE-9522057 and CHE-9526815).

Appendix A: Average Single-Molecule Line Shape

This appendix outlines the derivation of eqs 25 and 26. The starting point is eq 18, which we now average over all the TLS environments:

$$\langle I(\omega)\rangle = Re\left(\frac{1}{\pi}\int_0^\infty \mathrm{d}t\, \mathrm{e}^{\mathrm{i}\omega t}\mathrm{e}^{-t/2T_1}\langle\Phi_{\mathrm{SM}}(t)\rangle\right) \tag{A1}$$

where

$$\langle\Phi_{\mathrm{SM}}(t)\rangle = \langle \mathrm{e}^{-\mathrm{i}\int_0^t \mathrm{d}\tau\, \omega(\tau)}\rangle \tag{A2}$$

but now the angular brackets denote an average over all TLS environments as well as over the stochastic trajectories. The average now renders all of the TLS identical, and so we have

$$\langle\Phi_{\mathrm{SM}}(t)\rangle = \langle \mathrm{e}^{-\mathrm{i}\nu\int_0^t \mathrm{d}\tau\, \zeta(\tau)\Theta(K-1/\tau_{\mathrm{m}})}\rangle^N \tag{A3}$$

where N is the number of TLSs. For very large N this can be written as

$$\langle\Phi_{\mathrm{SM}}(t)\rangle = \exp[-N\langle(1-\mathrm{e}^{-\mathrm{i}\nu\int_0^t \mathrm{d}\tau\, \zeta(\tau)})\Theta(K-1/\tau_{\mathrm{m}})\rangle] \tag{A4}$$

The averages over the orientation parameter ϵ and TLS−chromophore distances r lead to[105,136]

$$\langle\Phi_{\mathrm{SM}}(t)\rangle = \exp\left[-\frac{4\pi^3}{3}\alpha\rho\left\langle\frac{A}{E}\int_0^t \mathrm{d}\tau\, \zeta(\tau)\Theta(K-1/\tau_{\mathrm{m}})\right\rangle\right] \tag{A5}$$

where in the above the thermodynamic limit $N \to \infty$, $r_{\mathrm{max}} \to \infty$, $N/(4\pi r_{\mathrm{max}}^3/3) = \rho$ (the TLS density) has been taken, and the remaining average is over the stochastic frequency trajectories and the TLS internal parameters. The former average involves only $\zeta(\tau)$, and since $\langle\zeta(\tau)\rangle = p$, we have simply

$$\langle\Phi_{\mathrm{SM}}(t)\rangle = \exp\left[-\frac{4\pi^3}{3}\alpha\rho t\left\langle\frac{A}{E}p\Theta(K-1/\tau_{\mathrm{m}})\right\rangle\right] \tag{A6}$$

where the remaining average is over the distributions of A and J. Writing A as $A = (E^2 - K/[cE\coth(\beta E/2)])^{1/2}$, it becomes convenient to convert the average over A and J to one over E and K. This gives[80,105]

$$\left\langle \frac{A}{E} p\Theta(K - 1/\tau_m) \right\rangle =$$

$$\frac{P_0}{2}\int_{J_{min}}^{\sqrt{A_{max}^2 + J_{max}^2}} dE \, \frac{E^\mu}{1 + e^{\beta E}} \int_{K_{max}(E)}^{K_{min}(E)} \frac{dK}{K}\left(1 - \frac{K}{K_{max}(E)}\right)^{\mu/2} \times \Theta(K - 1/\tau_m) \quad \text{(A7)}$$

where

$$P_0 = \frac{1 + \mu}{A_{max}^{1+\mu} \ln(J_{max}/J_{min})} \quad \text{(A8)}$$

$$K_{max}(E) = cE^3 \coth(\beta E/2) \quad \text{(A9)}$$

$$K_{min}(E) = cJ_{min}^2 E \coth(\beta E/2) \quad \text{(A10)}$$

Since $J_{min} \ll kT$, and $\sqrt{A_{max}^2 + J_{max}^2} \gg kT$, we can set the lower and upper limits of the E integral to 0 and ∞, respectively. Furthermore, since $K_{min}(E) < 1/\tau_m$ for all $E \sim$ kT, we can set the lower limit of the K integral to 0. Now changing variables such that $z = E/kT$ and $x = K\tau_m$, we can write

$$\langle \Phi_{SM}(t) \rangle = e^{-\gamma' t} \quad \text{(A11)}$$

where

$$\gamma' = \frac{2\pi^3}{3}\alpha\rho P_0 (kT)^{1+\mu} \int_0^\infty dz \, \frac{z^\mu}{1 + e^z} \int_0^{\Gamma_m z^3 \coth(z/2)} \times \frac{dx}{x}\left(1 - \frac{x}{\Gamma_m z^3 \coth(z/2)}\right)^{\mu/2} \Theta(x - 1) \quad \text{(A12)}$$

and $\Gamma_m = c(kT)^3\tau_m$. Finally, one can perform the Fourier transform to get

$$\langle I(\omega) \rangle = \frac{\gamma/\pi}{\omega^2 + \gamma^2} \quad \text{(A13)}$$

where $\gamma = 1/2T_1 + \gamma'$.

Appendix B: Determining the Two-Level System Density

The TLS spectral density $n_s(E)$ is the number of TLS per unit energy per unit volume. It is related to the TLS density ρ (number per unit volume) by

$$n_s(E) = \rho P(E) \quad \text{(B1)}$$

where $P(E)$ is the probability of obtaining a TLS with a given energy E. This can be obtained from the distributions of A and J by

$$P(E) = P_0 \int_0^{A_{max}} dA \int_{J_{min}}^{J_{max}} dJ \frac{A^\mu}{J} \delta(E - \sqrt{A^2 + J^2}) \quad \text{(B2)}$$

where P_0 is given by eq A8. For $J_{min} < E < J_{max}$ this is

$$P(E) = P_0 E^\mu \int_0^{\sqrt{1 - (J_{min}/E)^2}} \frac{x^\mu}{1 - x^2} \quad \text{(B3)}$$

Taking $\mu = 1/3$, this integral can be performed analytically, and assuming that $E \gg J_{min}$, gives

$$P(E) = P_0 E^{1/3} \ln\left(1.4485 \frac{E}{J_{min}}\right) \quad \text{(B4)}$$

The TLS density ρ_P quoted in ref 74 is actually

$$\rho_P = \int_{0.5kK}^{1.5kK} dE \, n_s(E) \quad \text{(B5)}$$

From eq B1 we then have

$$\rho = \frac{\rho_P}{\int_{0.5kK}^{1.5kK} dE \, P(E)} \quad \text{(B6)}$$

Using

$$\int dE \, E^{1/3} \ln(\alpha E) = {}^9/_{16} E^{4/3} ({}^4/_3 \ln(\alpha E) - 1) \quad \text{(B7)}$$

and the parameter values of $A_{max}/k = J_{max}/k = 17$ K and $J_{min}/k = 2.76 \times 10^{-7}$ K gives

$$\int_{0.5kK}^{1.5kK} dE \, P(E) = 0.026 \quad \text{(B8)}$$

Finally, taking[74] $\rho_P = 3 \times 10^{-4}$ nm^{-3} gives $\rho = 1.15 \times 10^{-2}$ nm^{-3}.

References and Notes

(1) Skinner, J. L. *Annu. Rev. Phys. Chem.* **1988**, *39*, 463.
(2) Macfarlane, R. M.; Shelby, R. M. *J. Lumin.* **1987**, *7*, 179.
(3) Moerner, W. E. *Persistent Spectral Hole Burning: Science and Applications*; Springer-Verlag: Berlin, 1988.
(4) Narasimhan, L. R.; Littau, K. A.; Pack, D. W.; Bai, Y. S.; Elschner, A.; Fayer, M. D. *Chem. Rev.* **1990**, *90*, 439.
(5) Skinner, J. L.; Moerner, W. E. *J. Phys. Chem.* **1996**, *100*, 13251.
(6) Stoneham, A. M. *Rev. Mod. Phys.* **1969**, *41*, 82.
(7) Sevian, H. M.; Skinner, J. L. *Theor. Chim. Acta* **1992**, *82*, 29.
(8) Sevian, H. M.; Skinner, J. L. *J. Chem. Phys.* **1992**, *97*, 8.
(9) Orth, D. L.; Mashl, R. J.; Skinner, J. L. *J. Phys.: Condens. Matter* **1993**, *5*, 2533.
(10) Kharlamov, B. M.; Personov, R. I.; Bykovskaya, L. A. *Opt. Commun.* **1974**, *12*, 191.
(11) Haarer, D.; Silbey, R. *Phys, Today* **1990**, *May*, 58.
(12) Szabo, A. *Phys. Rev. Lett.* **1970**, *25*, 924.
(13) Kurnit, N. A.; Abella, I. D.; Hartmann, S. R. *Phys. Rev. Lett.* **1964**, *13*, 567.
(14) Allen, L.; Eberly, J. *Optical Resonance and Two-Level Atoms*; Dover: New York, 1987.
(15) Narasimhan, L. R.; Bai, Y. S.; Dugan, M. A.; Fayer, M. D. *Chem. Phys. Lett.* **1991**, *176*, 335.
(16) Meijers, H. C.; Wiersma, D. A. *Phys. Rev. Lett.* **1992**, *68*, 381.
(17) Asaka, S.; Nakatsuka, H.; Fujiwara, M.; Matsuoka, M. *Phys. Rev. A* **1984**, *29*, 2286.
(18) Morita, N.; Yajima, T. *Phys. Rev. A* **1984**, *30*, 2525.
(19) Beach, R.; Hartmann, R. *Phys. Rev. Lett.* **1984**, *53*, 663.
(20) Hesselink, W. H.; Wiersma, D. A. *Phys. Rev. Lett.* **1979**, *43*, 1991.
(21) Hesselink, W. H.; Wiersma, D. A. *J. Chem. Phys.* **1981**, *75*, 4192.
(22) Hsu, D.; Skinner, J. L. *J. Chem. Phys.* **1984**, *81*, 5471.
(23) Hsu, D.; Skinner, J. L. *J. Chem. Phys.* **1985**, *83*, 2097.
(24) Hsu, D.; Skinner, J. L. *J. Chem. Phys.* **1985**, *83*, 2107.
(25) Moerner, W. E.; Kador, L. *Phys. Rev. Lett.* **1989**, *62*, 2535.
(26) Orrit, M.; Bernard, J. *Phys. Rev. Lett.* **1990**, *65*, 2716.
(27) Moerner, W. E.; Basché, T. *Angew. Chem.* **1993**, *32*, 457.
(28) Orrit, M.; Bernard, J.; Personov, R. I. *J. Phys. Chem.* **1993**, *97*, 10256.
(29) Moerner, W. E. *J. Lumin.* **1994**, *60*, 997.
(30) Moerner, W. E. *Science* **1994**, *265*, 46.
(31) Basché, T.; Moerner, W.; Orrit, M.; U. P. Wild, E. *Single-Molecule Optical Detection, Imaging, and Spectroscopy;* VCH: Weinheim, 1996.
(32) Moerner, W. E. *Acc. Chem. Res.* **1996**, *29*, 563.
(33) Ambrose, W. P.; Moerner, W. E. *Nature* **1991**, *349*, 225.
(34) Ambrose, W. P.; Basché, T.; Moerner, W. E. *J. Chem. Phys.* **1991**, *95*, 7150.
(35) Ambrose, W. P.; Basché, T.; Moerner, W. E. *J. Lumin.* **1992**, *53*, 62.
(36) Basché, T.; Moerner, W. E.; Orrit, M.; Tallon, H. *Phys. Rev. Lett.* **1992**, *69*, 1516.
(37) Talon, H.; Fleury, L.; Bernard, J.; Orrrit, M. *J. Opt. Soc. Am. B* **1992**, *9*, 825.
(38) Bernard, J.; Fleury, L.; Orrit, M.; Talon, H.; Orrit, M. *J. Chem. Phys.* **1993**, *98*, 850.
(39) Croci, M.; Muschenborn, H. J.; Guttler, F.; Renn, A.; Wild, U. P. *Chem. Phys. Lett.* **1993**, *212*, 71.
(40) Guttler, F.; Sepiol, J.; Plakhotnik, T.; Mitterdorfer, A.; Renn, A.; Wild, U. P. *J. Lumin.* **1993**, *56*, 29.

(41) Pirotta, M.; Guttler, F.; Gygax, H.; Renn, A.; Sepiol, J.; Wild, U. P. *Chem. Phys. Lett.* **1993**, *208*, 379.
(42) Orrit, M.; Bernard, J.; Brown, R.; Fleury, L.; Wrachtrup, J.; von Borczyskowski, C. *J. Lumin.* **1994**, *60*, *61*, 991.
(43) Wild, U. P.; Croci, M.; Guttler, F.; Pirotta, M.; Renn, A. *J. Lumin.* **1994**, *60*, *61*, 1003.
(44) Wrachtrup, J.; von Borczyskowski, C.; Bernard, J.; Brown, R.; Orrit, M. *Chem. Phys. Lett.* **1995**, *245*, 262.
(45) Basché, T.; Kummer, S.; Bräuchle, B. *Nature* **1995**, *373*, 132.
(46) Köhler, J.; Brouwer, A. C. J.; Schmidt, E. J. J. *Science* **1995**, *268*, 1457.
(47) Müller, A.; Richter, W.; Kador, L. *Chem. Phys. Lett.* **1995**, *241*, 547.
(48) Jelezko, F.; Tamarat, Ph.; Lounis, B.; Orrit, M. *J. Phys. Chem.* **1996**, *100*, 13892.
(49) Moerner, W. E.; Plakhotnik, T.; Irngatinger, T.; Croci, M.; Palm, V.; Wild, U. P. *J. Phys. Chem.* **1994**, *98*, 7382.
(50) Plakhotnik, T.; Moerner, W. E.; Irngartinger, T.; Wild, U. P. *Chimia* **1994**, *48*, 31.
(51) Plakhotnik, T.; Walser, D.; Pirotta, M.; Renn, A.; Wild, U. P. *Science* **1996**, *271*, 1703.
(52) Plakhotnik, T.; Walser, D.; Renn, A.; Wild, U. P. *Phys. Rev. Lett.* **1996**, *77*, 5363.
(53) Irngartinger, T.; Renn, A.; Wild, U. P. *J. Lumin.* **1996**, *66*, *67*, 232.
(54) Pirotta, M.; Renn, A.; Werts, M. H. V.; Wild, U. P. *Chem. Phys. Lett.* **1996**, *250*, 576.
(55) Boiron, A. M.; Lounis, B.; Orrit, M. *J. Chem. Phys.* **1996**, *105*, 3939.
(56) Vacha, M.; Liu, Y.; Nakatsuka, H.; Tani, T. *Mol. Cryst. Liq. Cryst.* **1996**, *291*, 81.
(57) Vacha, M.; Liu, Y.; Nakatsuka, H.; Tani, T. *J. Chem. Phys.* **1997**, *106*, 8324.
(58) Kozankiewicz, B.; Bernard, J.; Orrit, M. *J. Chem. Phys.* **1994**, *101*, 9377.
(59) Kettner, R.; Tittel, J.; Basché, T.; Bräuchle, C. *J. Phys. Chem.* **1994**, *98*, 6671.
(60) Tittel, J.; Kettner, R.; Basché, T.; Bräuchle, C.; Quante, H.; Müllen, K. *J. Lumin.* **1995**, *64*, 1.
(61) Basché, T.; Ambrose, W. P.; Moerner, W. E. *J. Opt. Soc. Am. B* **1992**, *9*, 829.
(62) Basché, T.; Moerner, W. E. *Nature* **1992**, *355*, 335.
(63) Orrit, M.; Bernard, J.; Zumbusch, A.; Personov, R. I. *Chem. Phys. Lett.* **1992**, *196*, 595.
(64) Fleury, L.; Zumbusch, A.; Orrit, M.; Brown, R.; Bernard, J. *J. Lumin.* **1993**, *56*, 15.
(65) Tchénio, P.; Myers, A. B.; Moerner, W. E. *J. Lumin.* **1993**, *56*, 1.
(66) Zumbusch, A.; Fleury, L.; Brown, R.; Bernard, J.; Orrit, M. *Phys. Rev. Lett.* **1993**, *70*, 3584.
(67) Myers, A. B.; Tchenio, P.; Zgierski, M. Z.; Moerner, W. E. *J. Phys. Chem.* **1994**, *98*, 10377.
(68) Myers, A. B.; Tchenio, P.; Zgierski, M. Z.; Moerner, W. E. *J. Lumin.* **1994**, *58*, 161.
(69) Phillips, W. A. *Amorphous Solids. Low-Temperature Properties;* Springer-Verlag: Berlin, 1981.
(70) Phillips, W. A. In *Amorphous Solids and the Liquid State*; March, N., Street, R., Tosi, A., Eds.; Plenum Press: New York, 1985; p 467.
(71) Phillips, W. A. *Rep. Prog. Phys.* **1987**, *50*, 1657.
(72) Hunklinger, S.; Raychaudhuri, A. K. *Prog. Low Temp. Phys.* **1986**, *9*, 265.
(73) Zeller, R. C.; Pohl, R. O. *Phys. Rev. B* **1971**, *4*, 2029.
(74) Pohl, R. O. In *Amorphous solids. Low-temperature properties*; Phillips, W., Ed.; Springer-Verlag: Berlin, 1981; p 27.
(75) Anderson, A. C. In *Amorphous Solids. Low-Temperature Properties*; Phillips, W., Ed.; Springer-Verlag: Berlin, 1981; p 65.
(76) Golding, B.; Graebner, J. E.; Schutz, R. J. *Phys. Rev. B* **1976**, *14*, 1660.
(77) Black, J. L.; Halperin, B. I. *Phys. Rev. B* **1977**, *16*, 2879.
(78) Golding, B.; Graebner, J. E.; Halperin, B. I.; Schutz, R. J. *Phys. Rev. Lett.* **1973**, *30*, 223.
(79) Graebner, J. E.; Allen, L. C.; Golding, B.; Kane, A. B. *Phys. Rev. B* **1983**, *27*, 3697.
(80) Silbey, R.; Koedijk, J. M. A.; Völker, S. *J. Chem. Phys.* **1996**, *105*, 901.
(81) Yu, C. C.; Leggett, A. J. *Comments Condens. Matter. Phys.* **1988**, *14*, 231.
(82) Anderson, P. W.; Halperin, B. I.; Varma, C. M. *Philos. Mag.* **1971**, *25*, 1.
(83) Phillips, W. A. *J. Low. Temp. Phys.* **1972**, *7*, 351.
(84) Jäckle, J. *Z. Phys.* **1972**, *257*, 212.
(85) Golding, B.; Graebner, J. E. *Phys. Rev. Lett.* **1976**, *37*, 852.
(86) Hunklinger, S.; Schickfus, M. V. In *Amorphous Solids. Low-Temperature Properties*; Phillips, W., Ed.; Springer-Verlag: Berlin, 1981; p 81.
(87) Jankowiak, R.; Hayes, J. M.; Small, G. J. *Chem. Rev.* **1993**, *93*, 1471.
(88) Klauder, J. R.; Anderson, P. W. *Phys. Rev.* **1962**, *125*, 912.
(89) Joffrin, J.; Levelut, A. *J. Phys. (Paris)* **1975**, *36*, 811.
(90) Arnold, W.; Hunklinger, S. *Solid State Commun.* **1975**, *17*, 883.
(91) Maynard, R.; Rammal, R.; Suchail, R. *J. Phys. Let.* **1980**, *41*, 291.
(92) Reinecke, T. L. *Solid State Commun.* **1979**, *32*, 1103.
(93) Hunklinger, S.; Schmidt, M. *Z. Phys. B* **1984**, *54*, 93.
(94) Berg, M.; Walsh, C. A.; Narasimhan, L. R.; Littau, K. A.; Fayer, M. D. *J. Chem. Phys.* **1988**, *88*, 1564.
(95) Huber, D. L.; Broer, M. M.; Golding, B. *Phys. Rev. Lett.* **1984**, *52*, 2281.
(96) Broer, M. M.; Golding, B.; Haemmerle, W. H.; Simpson, J. R.; Huber, D. L. *Phys. Rev. B* **1986**, *33*, 4160.
(97) Huber, D. L. *J. Lumin.* **1987**, *36*, 307.
(98) Putikka, W. O.; Huber, D. L. *Phys. Rev. B* **1987**, *36*, 3436.
(99) Bai, Y. S.; Fayer, M. D. *Chem. Phys.* **1988**, *128*, 135.
(100) Bai, Y. S.; Fayer, M. D. *Phys. Rev. B* **1988**, *37*, 1440.
(101) Bai, Y. S.; Fayer, M. D. *Phys. Rev. B* **1989**, *39*, 11066.
(102) Suárez, A.; Silbey, R. *Chem. Phys. Lett.* **1994**, *218*, 445.
(103) Geva, E.; Reilly, P. D.; Skinner, J. L. *Acc. Chem. Res.* **1996**, *29*, 579.
(104) Geva, E.; Skinner, J. L. *Mol. Cryst. Liq. Cryst.* **1996**, *291*, 73.
(105) Geva, E.; Skinner, J. L. *J. Chem. Phys.* **in press**.
(106) Heuer, A.; Silbey, R. *Phys. Rev. Lett.* **1993**, *70*, 3911.
(107) Heuer, A.; Silbey, R. *Phys. Rev. B* **1994**, *49*, 1441.
(108) Heuer, A.; Silbey, R. *Phys. Rev. B* **1996**, *53*, 1.
(109) Skinner, J. L.; Trommsdorf, H. P. *J. Chem. Phys.* **1988**, *89*, 897.
(110) Love, W. F. *Phys. Rev. Lett.* **1973**, *31*, 822.
(111) Fetter, A. L.; Walecka, J. D. *Quantum Theory of Many-Particle Systems;* McGraw-Hill: New York, 1971.
(112) Silbey, R.; Kassner, K. *J. Lumin.* **1987**, *36*, 283.
(113) Leggett, A. J.; Chakravarty, S.; Dorsey, A. T.; Fisher, M.; Garg, A.; Zwerger, W. *Rev. Mod. Phys.* **1987**, *59*, 1.
(114) Laird, B. B.; Budimir, J.; Skinner, J. L. *J. Chem. Phys.* **1991**, *94*, 4391.
(115) Black, J. L. *Phys. Rev. B* **1978**, *17*, 2740.
(116) Berret, J. F.; Meissner, M. *Z. Phys. B* **1988**, *70*, 65.
(117) Reilly, P. D.; Skinner, J. L. *Phys. Rev. Lett.* **1993**, *71*, 4257.
(118) Reilly, P. D.; Skinner, J. L. *J. Chem. Phys.* **1994**, *101*, 959.
(119) Reilly, P. D.; Skinner, J. L. *J. Chem. Phys.* **1994**, *101*, 965.
(120) Reilly, P. D.; Skinner, J. L. *J. Chem. Phys.* **1995**, *102*, 1540.
(121) Skinner, J. L. In *Single-Molecule Optical Detection, Imaging, and Spectroscopy*; Basché, T., Moerner, W., Orrit, M., Wild, U., Eds.; VCH: Weinheim, 1996; p 143.
(122) Abragam, A. *The Principles of Nuclear Magnetism;* Clarendon: Oxford, 1961.
(123) Slichter, C. P. *Principles of Magnetic Resonance;* Springer-Verlag: Berlin, 1990.
(124) Thijssen, H. P. H.; van den Berg, R.; Völker, S. *Chem. Phys. Lett.* **1983**, *97*, 295.
(125) Thijssen, H. P. H.; van den Berg, R.; Völker, S. *Chem. Phys. Lett.* **1983**, *103*, 23.
(126) Völker, S. *Annu. Rev. Phys. Chem.* **1989**, *40*, 499.
(127) Molenkamp, L. W.; Wiersma, D. A. *J. Chem. Phys.* **1985**, *83*, 1.
(128) Carter, T. P.; Small, G. J. *Chem. Phys. Lett.* **1985**, *120*, 178.
(129) Narasimhan, L. R.; Pack, D. W.; Fayer, M. D. *Chem. Phys. Lett.* **1988**, *152*, 287.
(130) Baer, B. J.; Chronister, E. L. *J. Chem. Phys.* **1995**, *103*, 9510.
(131) Maier, H.; Kharlamov, B. M.; Haarer, D. *Phys. Rev. Lett.* **1996**, *76*, 2085.
(132) Dab, D.; Heurer, A.; Silbey, R. J. *J. Lumin.* **1995**, *64*, 95.
(133) Kubo, R. *Adv. Chem. Phys.* **1969**, *15*, 101.
(134) Anderson, P. W. *J. Phys. Soc. Jpn.* **1954**, *9*, 316.
(135) Kubo, R. *J. Phys. Soc. Jpn.* **1954**, *6*, 935.
(136) Hu, P.; Walker, L. R. *Phys. Rev. B* **1978**, *18*, 1300.
(137) Abramowitz, M.; Stegun, I. A. *Handbook of Mathematical Functions;* Dover: New York, 1972.
(138) Meijers, H. C.; Wiersma, D. A. *J. Chem. Phys.* **1994**, *101*, 6927.
(139) Vainer, Y. G.; Personov, R. I.; Zilker, S.; Haarer, D. *Mol. Cryst. Liq. Cryst.* **1996**, *291*, 51.
(140) Zilker, S. J.; Giering, T.; Haarer, D.; Vainer, Y. G.; Personov, R. I. **Preprint**.
(141) Vainer, Y. G.; Plakhotnik, T. V.; Personov, R. I. *Chem. Phys.* **1996**, *209*, 101.
(142) Zimdars, D.; Fayer, M. D. *J. Chem. Phys.* **1996**, *104*, 3865.